ISSN 1674-1056
http://cpb.iphy.ac.cn
http://iopscience.iop.org/cpb
中国物理 B
Chinese Physics
中国物理 Chinese Physics B

Excellent thermal stability and thermoelectric properties of *Pnma*-phase SnSe in middle temperature aerobic environment

Yu Tang(唐语), Decong Li(李德聪), Zhong Chen(陈钟), Shuping Deng(邓书平), Luqi Sun(孙璐琪), Wenting Liu(刘文婷), Lanxian Shen(申兰先), Shukang Deng(邓书康)

Citation: Chin. Phys. B . 2018, 27(11): 118105. **doi:** 10.1088/1674-1056/27/118105
Journal homepage: http://cpb.iphy.ac.cn; http://iopscience.iop.org/cpb

What follows is a list of articles you may be interested in

High thermal stability of diamond-cBN-B_4C-Si composites

Hong-Sheng Jia(贾洪声), Pin-Wen Zhu(朱品文), Hao Ye(叶灏), Bin Zuo(左斌), Yuan-Long E(鄂元龙), Shi-Chong Xu(徐仕翀), Ji Li(李季), Hai-Bo Li(李海波), Xiao-Peng Jia(贾晓鹏), Hong-An Ma(马红安)
Chin. Phys. B . 2017, 26(1): 018102. **doi:** 10.1088/1674-1056/26/1/018102

Influences of annealing on structural and compositional properties of Al_2O_3 thin films grown on 4H-SiC by atomic layer deposition

Li-Xin Tian(田丽欣), Feng Zhang(张峰), Zhan-Wei Shen(申占伟), Guo-Guo Yan(闫果果), Xing-Fang Liu(刘兴昉), Wan-Shun Zhao(赵万顺), Lei Wang(王雷), Guo-Sheng Sun(孙国胜), Yi-Ping Zeng(曾一平)
Chin. Phys. B . 2016, 25(12): 128104. **doi:** 10.1088/1674-1056/25/12/128104

Low specific contact resistivity to graphene achieved by AuGe/Ni/Au and annealing process

Shu-Zhen Yu(于淑珍), Yan Song(宋焱), Jian-Rong Dong(董建荣), Yu-Run Sun(孙玉润), Yong-Ming Zhao(赵勇明), Yang He(何洋)
Chin. Phys. B . 2016, 25(11): 118101. **doi:** 10.1088/1674-1056/25/11/118101

Fluctuations of electrical and mechanical properties of diamond induced by interstitial hydrogen

Zhuang Chun-Qiang, Liu Lei
Chin. Phys. B . 2015, 24(1): 018101. **doi:** 10.1088/1674-1056/24/1/018101

Thermal stability and high-temperature shape memory characteristics of Ti-20Zr-10Ta alloy

Zheng Xiao-Hang, Sui Jie-He, Zhang Xin, Yang Zhe-Yi, Cai Wei
Chin. Phys. B . 2014, 23(1): 018101. **doi:** 10.1088/1674-1056/23/1/018101

Excellent thermal stability and thermoelectric properties of $Pnma$-phase SnSe in middle temperature aerobic environment*

Yu Tang(唐语)[1], Decong Li(李德聪)[1,2], Zhong Chen(陈钟)[1], Shuping Deng(邓书平)[1], Luqi Sun(孙璐琪)[1], Wenting Liu(刘文婷)[1], Lanxian Shen(申兰先)[1], and Shukang Deng(邓书康)[1,†]

[1] *Education Ministry Key Laboratory of Renewable Energy Advanced Materials and Manufacturing Technology, Yunnan Normal University, Kunming* 650500, *China*

[2] *Photoelectric Engineering College, Yunnan Open University, Kunming* 650500, *China*

(Received 3 July 2018; revised manuscript received 10 August 2018; published online 19 October 2018)

SnSe is considered to be a promising thermoelectric material due to a high ZT value and abundant and non-toxic composition elements. However, the thermal stability is an important issue for commercial application. In particular, thermoelectric materials are in the high temperature for a long time due to the working condition. The present work investigates the thermal stability and oxidation resistance of single crystal SnSe thermoelectric materials. The scanning electron microscopy (SEM) and transmission electron microscopy (TEM) results show that the internal of SnSe crystal is not easily oxidized, while the x-ray photoelectron spectroscopy (XPS) results indicate that the surface of SnSe is slight oxidized to SnO_2. Even if the surface is oxidized, the SnSe crystal still exhibits stable thermoelectric properties. Meanwhile, the crystallization quality of SnSe samples can be improved after the appropriate heat treatment in the air, which is in favor of the carrier mobility and can improve the electrical conduction properties of SnSe. Moreover, the decrease of defect density after heat treatment can further improve the Seebeck coefficient and electrical transport properties of SnSe. The density functional theory (DFT) calculation verifies the important role of defect on the electrical conductivity and electron configuration. In summary, appropriate temperature annealing is an effective way to improve the transmission properties of SnSe single crystal thermoelectric materials.

Keywords: SnSe, thermal stability, annealing, electrical transport properties, density functional theory

PACS: 81.05.Hd,72.20.Pa, 81.40.Ef, 31.15.es **DOI:** 10.1088/1674-1056/27/11/118105

1. Introduction

Thermoelectric devices can directly convert heat energy into electric energy, which provides an alternative method to replace fossil energy. The conversion efficiency of thermoelectric devices mainly depends on the properties of thermoelectric materials. The thermoelectric property of thermoelectric materials is determined by the dimensionless figure of merit, $ZT = (\alpha^2\sigma/\kappa)T$, where α, σ, κ, and T are the Seebeck coefficient, electrical conductivity, thermal conductivity, and absolute temperature, respectively.[1–7] According to the Pisarenko relations, Seebeck coefficient α can be given by

$$\alpha = \frac{8\pi^2 k_B^2}{3eh^2} m^* T \left(\frac{\pi}{3n}\right)^{2/3}, \quad (1)$$

where k_B is the Boltzmann constant, e is the electron charge, h is the Plank constant, and m^* is the effective mass of carriers.[8] Some studies have suggested that the threshold of commercial application of thermoelectric materials is that the ZT value is above 3.[9] In recent years, a large number of studies have been carried out to improve the ZT value of thermoelectric materials.[10–15]

SnSe is a potential thermoelectric material that has increasingly attracted attention due to its high ZT value and the abundant and non-toxic composition elements.[16–18] As shown in Fig. 1(a), low-temperature phase single crystal SnSe has an anisotropic layered orthorhombic crystal structure.[19–21] The two atom-thick SnSe slabs are strongly corrugated, creating a zig-zag folded accordion-like projection along the b-axis, which decides their extraordinary electronic structures. As shown in Figs. 1(b)–1(d), there is a heavy-mass band along YT direction, which is expected to give a high Seebeck coefficient.[22] Meanwhile, SnSe maintains an ultralow thermal conductivity owing to the strong anharmonic bonding.[23–30] The ZT value of single crystal SnSe can reach 2.6 at 923 K, which makes SnSe a popular research topic in thermoelectric materials.[12] However, many problems still need to be studied to realize wide application of SnSe. For example, the phase transition from *Pnma* to *Cmcm* is required to obtain the high ZT value of 2.6 for single crystal SnSe thermoelectric materials.[31,32] Moreover, thermal stability is an important parameter for commercial application. Especially, materials are easily oxidized under the high temperature conditions of the thermoelectric materials process. Besides, the thermoelectric properties of SnSe at moderate and low temperature scales need to be further improved.[33] Many studies have been devoted to improving the thermoelectric properties of SnSe at moderate and low temperatures.[34–40] For example, the ZT value of Na-doped SnSe can be as high as 2.0 and

*Project supported by the National Natural Science Foundation of China (Grant No. 61864012).

†Corresponding author. E-mail: skdeng@126.com

© 2018 Chinese Physical Society and IOP Publishing Ltd

Bi-doped SnSe reached 2.2.[41] Chang *et al.*[42] synthesized n-type Br-doped polycrystalline SnSe with high *ZT* value of ~ 1.2 at 773 K; Peng *et al.*[43] reported that the average *ZT* value is higher than 1.17 along the crystallographic *b*-axis of Na-doped SnSe, with the maximum *ZT* reaching a value of 2 at 800 K; Zhang *et al.*[44] induced strain into SnSe by pressuring and *ZT* values of p-type along the *b* and *c* directions can reach as high as 2.5 and 1.7 at 6 GPa and 700 K, respectively. As a promising thermoelectric material, SnSe not only needs to have a high *ZT* value but should also have good thermal stability and oxidation resistance. Zhang *et al.*[45] studied the oxidation resistance of single crystal SnSe. It was found that the second amorphous $Sn_{1-x}Se$ alloy layer appeared in the thin amorphous oxide layer (mainly a-SnO_2) after long exposure to air at room temperature. Their results show that the amorphous alloy $Sn_{1-x}Se$ is a metastable phase, which will decompose and even evolve into the crystalline SnSe and $SnSe_2$. Thermoelectric materials often work in moderate and high temperature environments, and temperature has practical significance in the study of thermoelectric stability. In the previous studies, Li *et al.*[46] paid attention to the oxidation resistance of *Cmcm* phase SnSe at high temperature and found that SnSe is prone to oxidation at high temperature. However, the thermal stability of single crystal *Pnma* phase SnSe and the effect of oxygen on its thermoelectric properties have not been reported. Therefore, this paper focuses on the thermal stability of *Pnma* phase SnSe and the effect of oxidation on its thermoelectric properties.

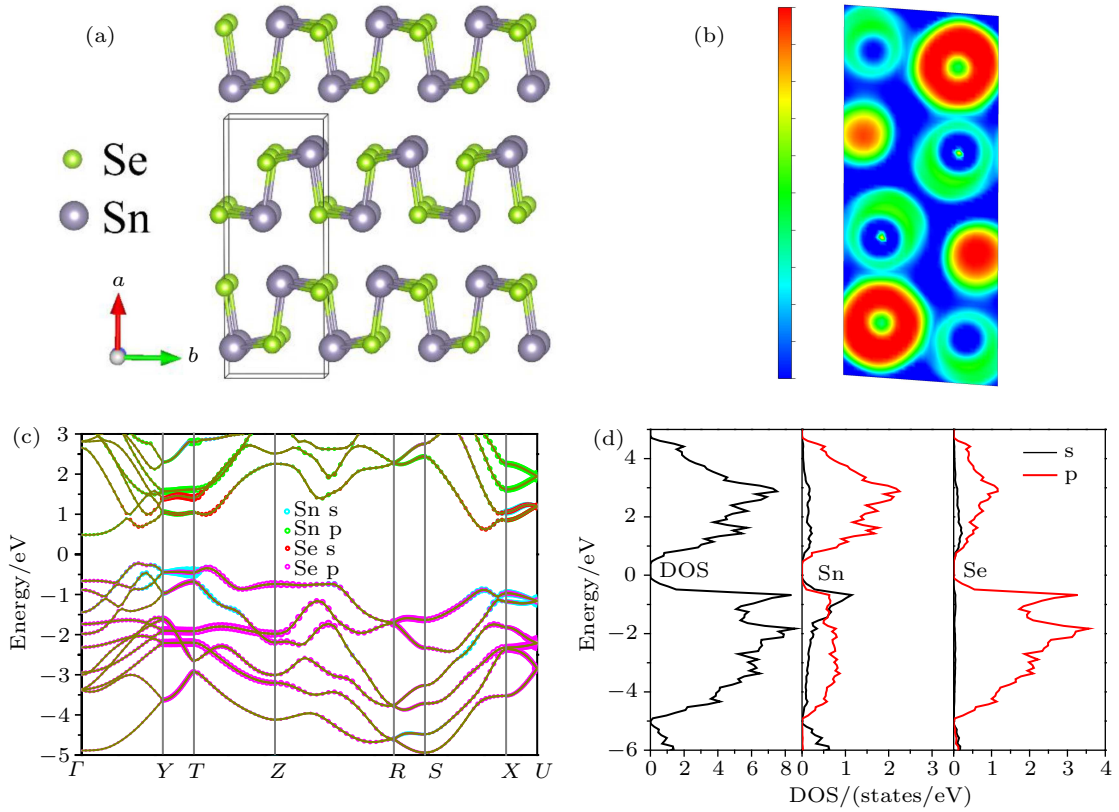


Fig. 1. (color online) (a) Crystal structure of the low-temperature *Pnma* phase of SnSe. (b) The electronic localization function (ELF) contour maps of SnSe. (c) The band structure of SnSe. (d) The DOS and PDOS of SnSe.

To explore whether the thermal stability and oxidation resistance of SnSe thermoelectric materials meet the requirements of practical application, it is necessary to carry out research on this issue. In this paper, single crystal SnSe thermoelectric material was prepared by Sn self-flux method. Subsequently, the prepared SnSe single crystal samples were heated continuously and repeatedly in air. The crystal structure, elementary composition, and electrical transport characteristics of heated SnSe were characterized. The results of each heated sample were compared and analyzed to explore the effect of heat treatment and oxidation on the thermoelectric properties of single crystal SnSe thermoelectric materials.

2. Experiment

High-purity elements Sn (99.999% ingot) and Se (99.99% powder) were weighed in accordance with their atomic ratios as Sn:Se = 4.5. Subsequently, the mixture was sealed in a vacuum quartz tube and heated in a rate 180 K/h ramp to 1173 K, incubated at this temperature for 10 h, then cooled down to 1023 K in 15 min and warmed up to 1123 K in 5 min. Af-

ter 1 h of incubation, the sample was slowly cooled down to 773 K over 80 h. At this temperature, the single crystals were separated from the molten Sn flux by the centrifuge. For easy measurement, we cut and polished the sample into the shape shown in Fig. 2(b) and named it S1.

Powder x-ray diffraction (XRD) with Cu $K\alpha$ radiation (Ultima IV) was used to analyze the crystal structures of S1. The lattice structure of S1 was observed through high-resolution transmission electron microscope (TEM). The surface morphologies were observed by scanning electron microscope (SEM). After polishing the sample (removing the surface layer), the inner chemical components of the sample were obtained by energy dispersive spectroscopy (EDS) test. To determine the chemical state of the sample, x-ray photoelectron spectroscopy (XPS) was performed. Electrical conductivity σ and Seebeck coefficient α were measured in the temperature range of 300–690 K in vacuum. Electrical conductivity σ was measured by a direct current (DC) four-probe method, and the DC current was kept at 20 mA. Seebeck coefficient α was measured by a comparative method, and constant (Ni: 40%) was used as a reference sample, of which α in the measured temperature range is known. Hall coefficients ($R_{\rm H}$) were measured by a Hall system (Nanometrics HL5500 Hall System) at room temperature (RT) in a magnetic field of 0.75 T. After those characterizations, S1 was subjected to the first heat-treatment at 523 K and the second heat-treatment at 573 K for 24 h each time. The samples were named S2 and S3 respectively after the two heat-treatments. The Seebeck coefficient, conductivity, elemental composition, Hall coefficient, and lattice structure were all characterized by the same method as S1. The characterization results of each heating sample were compared to explore the effect of long time heat-treatment on the electrical transport characteristics of SnSe thermoelectric materials and to study the thermal stability of SnSe thermoelectric materials.

Density functional theory (DFT) calculations were performed with the Vienna *ab-initio* simulation package (VASP).[47,48] The interaction between the core ion and valence electron was described by the projector augmented wave method (PAW).[49] The exchange correlation part was described with the spin-polarized generalized gradient approximations (GGA) in the scheme of Perdew, Burke, and Ernzerhof (PBE).[50,51] An energy cutoff of 500 eV was used with Monkhorst *k*-points[52] sampling scheme ($2\times5\times5$) for geometry optimization, while a larger grid $4\times10\times10$ was used for electronic structure computation. Conjugated gradient method was used to the geometry optimization and all the atomic coordinates were fully relaxed until the maximal force on each atom was less than 0.02 eV/Å, and the convergence condition for energy was 10^{-4} eV.

3. Results and discussion

To investigate the effects of high temperature and oxygen on single crystal SnSe heated in air, the surface morphology and elemental composition of SnSe before and after annealing were investigated by XRD and SEM equipped EDS. Figure 2(a) shows the XRD of the SnSe samples heated in air. All of the diffraction peaks of the prepared single crystal SnSe sample can be indexed by orthorhombic SnSe phase (space group *Pnma*, JCPDS: 48-1224), no other phases are observed within the detection limits of the measurements. After repeated heat-treatment for a long time, the diffraction peak angle of the samples remains the same and the relative diffraction intensity increases, which suggest that SnSe single crystals have good thermal stabilities. The enhancement of XRD diffraction peak intensity indicates that heat-treatment may help to improve the crystallization quality of SnSe. To further verify this conjecture, TEM was used to observe the lattice structure of S1 and S3. Figures 2(e) and 2(f) present the TEM images of S1 and S3. From S1 to S3, the lattice structure of the sample becomes neater and the number of dislocations decreases, which show that heat-treatment can improve the crystallization quality of SnSe. The improvement of crystal quality may be due to the annealing effect of 523573 K heat-treatment.

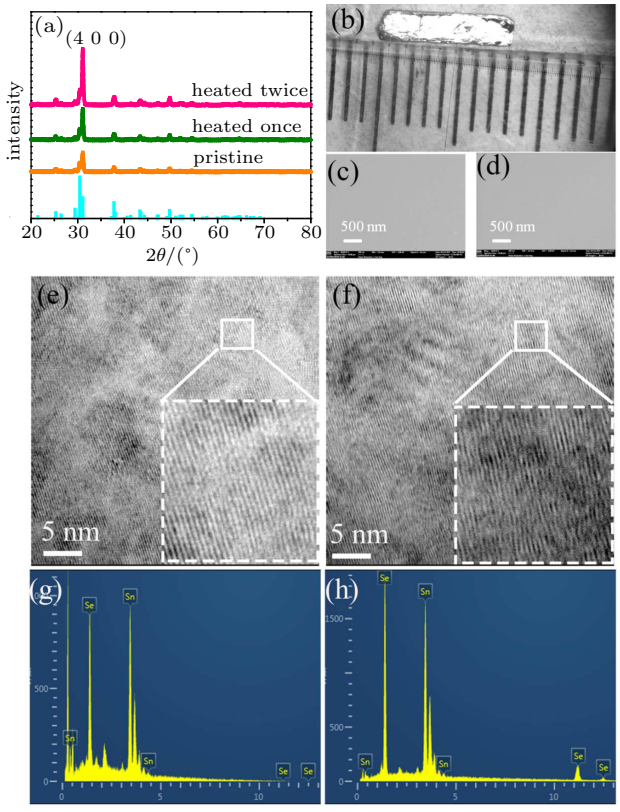


Fig. 2. (color online) (a) Powder x-ray diffraction patterns for all samples. (b) As grown and polished single crystal of SnSe. (c), (d) The SEM images of S1 and S3. (e), (f) The TEM images of S1 and S3. (g), (h) The EDS spectra of S1 and S3.

Figures 2(c) and 2(d) show the surface morphology images of S1 and S3, respectively. It can be seen from the SEM images that the surface morphology of the samples has not changed obviously before and after heat-treatment. EDS spectra of the sample after two heat-treatments are showed in Figs. 2(g) and 2(h). The percentage of the polished sample components measured by EDS is shown in Table 1. After two aerobic heat-treatments, there is no oxygen diffraction peak in the EDS spectra, indicating that internal of the SnSe crystal is not easy to be oxidized. The x-ray photoelectron spectroscopy (XPS) was performed to investigate the surface state after heat-treatments. The XPS spectrum in Fig. 3(a) shows the presence of Sn, Se, and O, confirming the presence of O. The Sn $3d_{3/2}$ and Sn $3d_{5/2}$ orbital peaks for SnSe are observed at 494.0 eV and 485.6 eV, respectively. Meanwhile, the peaks also appear at slightly higher binding energies of 494.9 eV and 486.6 eV, which correspond to SnO_2. Thus, part SnSe is oxidized to SnO_2. Quantifying the peaks suggests the composition of SnO_2: SnSe of 1:2, indicating that a small part of surface SnSe is oxidized and the oxidation is not serious.

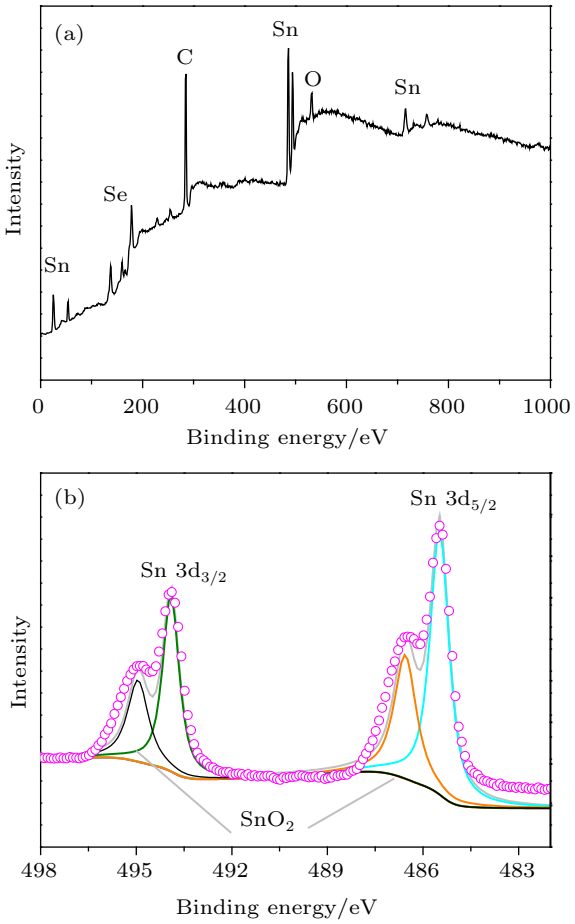


Fig. 3. (color online) (a) XPS spectrum of SnSe, (b) high-resolution scan for Sn.

Figure 4(a) shows the differential thermal analysis (DTA) of the prepared SnSe single crystal (S1). It can be seen from the diagram that the mass decay of SnSe is very small during the heating process, except for the melting peak of Sn that remains on the surface of the sample in a small amount at 505 K and the phase transition peak of SnSe from *Pnma* phase to *Cmcm* phase at 803 K, no miscellaneous peaks appear.

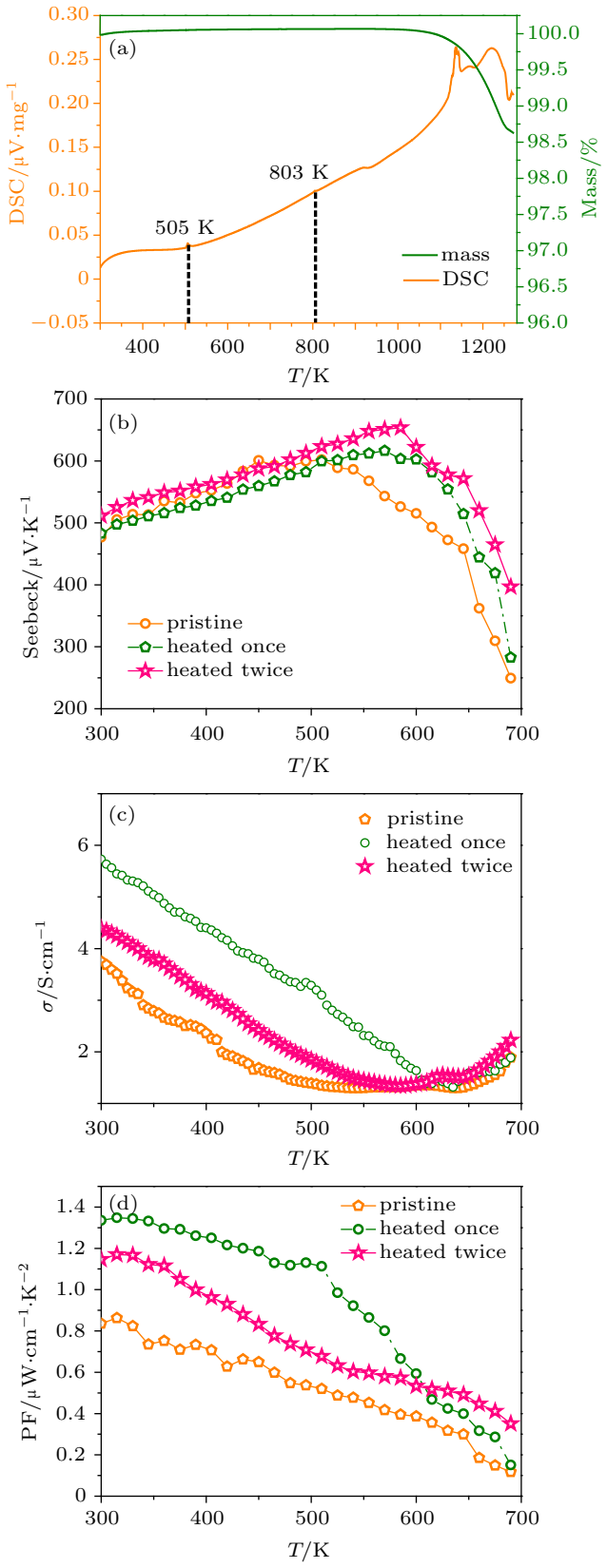


Fig. 4. (color online) (a) The DTA of S1 and (b) Seebeck coefficient α, (c) electrical conductivity σ, (d) power factor PF as functions of the temperature for all samples along the *c* axis.

After each annealing in the air atmosphere, the Seebeck coefficient and the electrical conductivity of the sample were measured. The measured results and the calculated power factors are shown in Fig. 4. By comparing the results of each test, we investigated the effect of annealing on the electrical transmission properties of SnSe single crystal thermoelectric materials. Figure 4(b) shows the temperature dependence of Seebeck coefficient for the prepared SnSe sample without heat-treatment and after each heat-treatment in aerobic environment. The Seebeck coefficient of the sample without heat-treatment is the lowest, about 476 μV/K at room temperature and 620 μV/K at 450 K. After the first heat-treatment at 523 K, the Seebeck coefficient is slightly increased to 482 μV/K at room temperature. As the temperature is increased to 570 K, the Seebeck coefficient grows to 616 μV/K, and it is higher than that of the sample without heat-treatment. After the second heat-treatment at 573 K, the Seebeck coefficient is further increased to 511 μV/K at room temperature, and the maximum value is 653 μV/K at 585 K. Figure 4(c) shows the temperature dependence of electrical conductivity for the as-grown and the heat treatment samples in aerobic environment. It can be seen from the diagram that before 580 K, the electrical conductivity of all samples decreases with the increase of temperature, and increases gradually after this temperature. By comparing the electrical conductivity of each heat-treatment sample, it is found that heating treatment can significantly enhance the electrical conductivity of SnSe. In particular, the first heat-treatment at 523 K increases the electrical conductivity of the samples by 53% (from 3.75 S/cm to 5.73 S/cm at room temperature). However, after the second heat-treatment at 573 K, the electrical conductivity of the sample decreases obviously, and the electrical conductivity is 4.38 S/cm at room temperature. The relation between the power factor calculated from $\mathrm{PF} = \alpha^2\sigma$ and temperature is shown in Fig. 4(d). The first heat-treatment of SnSe increases its power factor from 0.83 $\mu\mathrm{W\cdot cm^{-1}\cdot K^{-2}}$ to 1.33 $\mu\mathrm{W\cdot cm^{-1}\cdot K^{-2}}$ at room temperature and its maximum value is close to 1.35 $\mu\mathrm{W\cdot cm^{-1}\cdot K^{-2}}$ at 315 K. After the second heat-treatment, the power factor at room temperature decreases to 1.15 $\mu\mathrm{W\cdot cm^{-1}\cdot K^{-2}}$ due to the decrease of the electrical conductivity of the sample, and the maximum value appears at 315 K, which is 1.17 $\mu\mathrm{W\cdot cm^{-1}\cdot K^{-2}}$.

To explore this phenomenon, Hall coefficient R_H was measured at room temperature. As shown in Table 1, the Hall coefficients of the samples before and after heat-treatment are all positive, and the heat-treatment has a significant effect on the Hall coefficients of the samples. The Hall coefficient of the sample increases from 1.5×10^{-5} $\mathrm{m^3/C}$ to 2.6×10^{-5} $\mathrm{m^3/C}$. Based on the results of Hall coefficient and electrical conductivity measurements, we calculated the carrier concentration and mobility at room temperature by $\mu_\mathrm{H} = |R_\mathrm{H}|\sigma$ and $n = \sigma/e\mu_\mathrm{H}$ for the heat-treatment samples. As shown in Table 1, the carrier concentration of the pristine sample is the highest (4.2×10^{17} $\mathrm{cm^{-3}}$) but its mobility is extremely low (56.2 $\mathrm{cm^2/V\cdot s}$). After the first annealing, the carrier concentration of the sample decreases by 16.7% to 3.5×10^{17} $\mathrm{cm^{-3}}$, while the carrier mobility increases significantly to 119.5 $\mathrm{cm^2/V\cdot s}$. After the second annealing, the carrier concentration decreases to 2.4×10^{17} $\mathrm{cm^{-3}}$ and the carrier mobility increases to 120.4 $\mathrm{cm^2/V\cdot s}$. From these results, it can be seen that annealing helps to improve the electrical transport characteristics of SnSe.

The reasons for the enhancement in electrical transport properties of the heat-treatment sample can be explained as follows. First, many defects exist in the as-grown SnSe crystal, which result in the high carrier concentration and the extremely low mobility of S1, and consequently the poor electrical conductivity. Second, after the first annealing, the number of defects in the SnSe crystal is reduced and the lattice structure is more complete, which lead to the increase of carrier mobility while the carrier concentration decreases. The contribution to the electrical conductivity due to the increased carrier mobility exceeds that due to the decreased carrier concentration, so the electrical conductivity of S2 is higher than that of S1. Third, in the second annealing treatment, attribute to the recrystallizing of SnSe, the elemental composition of the sample is closer to the stoichiometric ratio, as shown in Table 1, which makes the carrier concentration decrease further. Comparing with the as-grown sample, the improved crystallization quality reduces the carrier recombination and increases the carrier mobility, so the electrical conductivity is slightly improved.

According to formula (1), we can see that the high carrier concentration is not conducive to improving the Seebeck coefficient of thermoelectric materials. Annealing improves the crystal quality by reducing the number of defects in the SnSe crystal and improves the carrier mobility of the sample while reducing the carrier concentration. At the same time, the Seebeck coefficient of SnSe is also increased with the decrease of the carrier concentration.

Table 1. Crystal compositions (EDS), Hall coefficient R_H, carrier mobility μ_H, carrier density n, and electrical conductivity σ at room temperature for all samples.

Sample	Element compositions			$R_\mathrm{H}/10^{-5}$ $\mathrm{m^3\cdot C^{-1}}$	$\mu_\mathrm{H}/\mathrm{cm^2\cdot V^{-1}\cdot s^{-1}}$	$N/10^{17}$ $\mathrm{cm^{-3}}$	$\sigma/\mathrm{S\cdot cm^{-1}}$
	Sn/%	Se/%	Sn:Se				
Pristine	53.6	46.4	1.15	1.5	56.2	4.2	3.8
Heated once	53.1	46.9	1.13	1.8	119.5	3.5	6.7
Heated twice	52.7	47.3	1.10	2.6	120.4	2.4	4.6

To reveal the effect of vacancy on the electrical conductivity of SnSe, we calculated the density of states of SnSe with different vacancies by density functional theory.[53] The types of vacancies in the samples are not clear and, therefore, the densities of states of Sn vacancy (V_{Sn}) and Se vacancy (V_{Se}) in the SnSe crystal were calculated. The total density of states and partial density of states of pristine SnSe, V_{Se}, and V_{Sn} are shown in Fig. 5. The pristine SnSe shows semiconductor property with a band gap of 0.65 eV. For V_{Se}, some impurity peaks are introduced near the valence-band maximum (VBM), indicating a p-type doping and resulting in the improvement of electrical conductivity. V_{Sn} does not change the overall DOS except for the upshift of the valence band, reducing the band gap, which is conducive to the electrical conductivity. Combined with the experimental results, it can be inferred that there may be a large number of V_{Se} in the as-grown SnSe sample, and an annealing treatment can effectively reduce the concentration of V_{Se}. For V_{Se}, a small narrow peak appears around the VBM, which is mainly contributed by Sn-5p states. For the Sn vacancy, the DOS near the valance band is mainly contributed by Se-4p states. Meanwhile, Sn-5p states play an important role in the states near the conduction band minimum. Figure 5(c) and 5(d) illustrate the ELF contour maps of V_{Se} and V_{Sn}. It can be seen that electrons spread over Sn atom for V_{Se}, indicating that the extra electrons are attributed to electrons returned back to Sn. It is in accordance with the introduced impurity level near VBM (Fig. 4(b)). Meanwhile, the much higher degree of electron delocalization in the vacancy than the pristine one indicates intensive charge transfer. When the crystalline quality of the prepared SnSe material is too low, we can improve the crystal quality by annealing treatment, thus increasing the power factor of SnSe. However, the contribution of vacancies to electrical conductivity indicates that proper crystal defects can improve the electrical conductivity of the materials. Therefore, proper annealing conditions are very important to improve the power factor of SnSe thermoelectric materials.

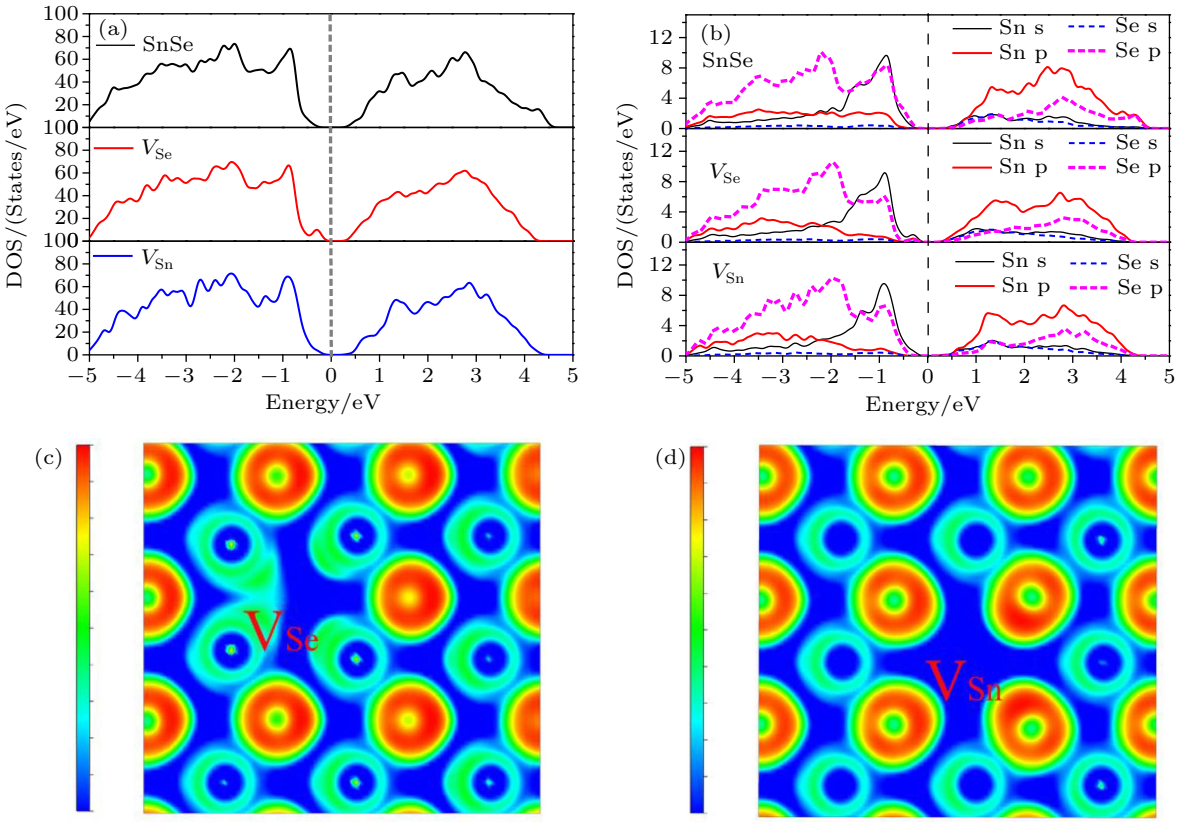


Fig. 5. (color online) (a) DOS, (b) PDOS, and (c), (d) ELF contour maps of Se and Sn vacancies.

4. Conclusion

The thermal stability is an important issue for thermoelectric materials due to the specific working condition. Herein, the thermal stability and oxidation resistance of single crystal SnSe thermoelectric materials prepared by Sn self-flux method were studied by repeated aerobic heating for a long time. The SEM and TEM results show that the internal of SnSe crystal cannot be easily oxidized; XPS results indicate that surface of SnSe is slightly oxidized to SnO_2. SnSe presents stable thermoelectric properties. Besides, the calculation and experimental results show that appropriate thermal treatment can improve the crystallization quality and reduce the defect density. Meanwhile, the decrease of defect density can improve the Seebeck coefficient. Unfortunately, the electrical conduc-

tivity will decrease with reduced carrier concentration. Therefore, an appropriate annealing is a key factor in balance the Seebeck coefficient and electrical conductivity of SnSe. In summary, the *Pnma*-phase single crystal SnSe presents excellent thermal stability and oxidation resistance, and annealing at appropriate temperature is an effective way to improve the transmission properties of SnSe single crystal thermoelectric materials.

References

[1] He J, Kanatzidis M G and Dravid V P 2013 *Mater. Today* **16** 166
[2] Kanatzidis M G 2010 *Chem. Mater.* **22** 648
[3] Li J F, Liu W S, Zhao L D, *et al.* 2010 *Npg Asia Mater.* **2** 152
[4] Minnich A J, Dresselhaus M S, Ren Z F and Chen G 2009 *Energy & Environmental Sci.* **2** 466
[5] Baxter J, Bian Z, Chen G, Danielson D, Dresselhaus M S, Fedorov A G, Fisher T S, Jones C W, Maginn E and Kortshagen U 2009 *Energy & Environmental Sci.* **2** 559
[6] Tan G, Zhao L D and Kanatzidis M G 2016 *Chem. Rev.* **116** 12123
[7] Popuri S R, Pollet M, Decourt R, Morrison F D, Bennett N S and Bos J W G 2016 *J. Mater. Chem. C* **4** 1685
[8] Zhang X and Zhao L D 2015 *J. Materiomics* **1** 92
[9] Wang F Q, Zhang S, Yu J, *et al.* 2015 *Nanoscale* **7** 15962
[10] Zhou Y, Zhao L D 2017 *Advanced Mater.* **29** 1702676
[11] Zhou B, Li S, Li W, Li J, Zhang X, Lin S, Chen Z and Pei Y 2017 *ACS Appl. Mater. Interfaces* **9** 34033
[12] Zhao L D, Lo S H, Zhang Y, Sun H, Tan G, Uher C, Wolverton C, Dravid V P and Kanatzidis M G 2014 *Nature* **508** 373
[13] Ding J, Xu B, Lin Y, Nan C and Liu W 2015 *New J. Phys.* **17** 083012
[14] Wei T R, Wu C F, Zhang X, Tan Q, Sun L, Pan Y and Li J F 2015 *Phys. Chem. Chem. Phys. Pccp* **17** 30102
[15] Harman T C, Taylor P J, Walsh M P and Laforge B E 2002 *Science* **297** 2229
[16] Agarwal A, Chaki S H and Lakshminarayana D 2007 *Mater. Lett.* **61** 5188
[17] Car R, Ciucci G and Quartapelle L 2010 *Phys. Status Solidi* **86** 471
[18] Dai X Q , Wang X L , Li W and Wang T X 2015 *Chin. Phys. B* **24** 117308
[19] Tang Y, Wang J, Li D, Deng S, Chen Z, Sun L, Liu W, Shen L and Deng S 2018 *J. Alloys & Compd.* **748** 80
[20] Makinistian L and Albanesi E A 2009 *Phys. Status Solidi* **246** 183
[21] Liu C Y, Miao L, Wang X Y, Wu S H, Zheng Y Y, Deng Z Y, Chen Y L, Wang G W and Zhou X Y 2018 *Chin. Phys. B* **27** 047211
[22] Tang Y, Cheng F, Li D C, Deng S P, Chen Z, Sun L Q, Liu W T, Shen L X and Deng S K 2018 *Physica B* **539** 8
[23] Wei T R, Wu C F, Zhang X, Tan Q, Sun L, Pan Y and Li J F 2015 *Phys. Chem. Chem. Phys.* **17** 30102
[24] Suzuki Y and Nakamura H 2015 *Phys. Chem. Chem. Phys.* **17** 29647
[25] Feng D, Ge Z H, Wu D, Chen Y X, Wu T, Li J and He J 2016 *Phys. Chem. Chem. Phys.* **18** 31821
[26] Huang L, Wu F and Li J 2016 *J. Chem. Phys.* **144** 114708
[27] Leng H Q , Zhou M, Zhao J, Han Y M and Li L F 2016 *RSC Adv.* **6** 9112
[28] Zhao L D , Chang C, Tan G and Kanatzidis M G 2016 *Energy & Environmental Sci.* **9** 3044
[29] Duvjir G, Min T, Thi Ly T, Kim T, Duong A T , Cho S, Rhim S H, Lee J and Kim J 2017 *Appl. Phys. Lett.* **110** 5227
[30] Agarwal A, Vashi M N, Lakshminarayana D and Batra N M 2000 *J. Mater. Sci. Mater. Electron.* **11** 67
[31] Mori H, Usui H, Ochi M and Kuroki K 2017 *Phys. Rev. B* **96** 085113
[32] Yang S D, Si J X, Su Q M and Wu H F2017 *Mater. Lett.* **193** 146
[33] Sava F, Borca C N, Galca A C, Socol G, Grolimund D, Mihai C and Velea A 2017 *Phys. Status Solidi* **255** 1700552
[34] Wu, D, *et al.* 2017 *Nano Energy* **35** 321
[35] Wang X, Xu J, Liu G Q, *et al.* 2017 *Npg Asia Mater.* **9** e426
[36] Sun Y, Wang D and Shuai Z 2017 *J. Phys. Chem. C* **121** 19080
[37] Xiao Y, Chang C, Zhang X, Pei Y, Li F, Yuan B, Gong S and Zhao L D 2016 *J. Mater. Sci.: Mater. Electron.* **27** 2712
[38] Chen Y X , Ge Z H , Yin M, Feng D, Huang X Q , Zhao W and He J 2016 *Advanced Funct. Mater.* **26** 6836
[39] Yan J J, Ke F, Liu C L, Wang L, Wang Q L, Zhang J K, Li G H, Han Y H, Ma Y Z and Gao C X 2016 *Phys. Chem. Chem. Phys.* **18** 5012
[40] Guo J, Jian J K, Liu J, Cao B L, Lei R B, Zhang Z H, Song B and Zhao H Z 2017 *Nano Energy* **38** 569
[41] Duong A T, *et al.* 2016 *Nat Commun.* **7** 13713
[42] Chang C, *et al.* 2016 *RSC Adv.* **6** 98216
[43] Peng K, Lu X, Zhan H, Hui S, Tang X, Wang G, Dai J, Uher C, Wang G and Zhou X 2016 *Energy & Environmental Sci.* **9** 454
[44] Zhang Y S, Hao S Q, Zhao L D , Wolverton C and Zeng Z 2016 *J. Mater. Chem. A* **4** 12073
[45] Zhang B, Peng K L, Sha X C, Li A, Zhou X Y, Chen Y H, Deng Q S, Yang D F, Ma E and Han X D2017 *Microscopy & Microanalysis* **23** 173
[46] Li Y, He B, Heremans J P and Zhao J C 2016 *J. Alloys Compd.* **669** 224
[47] Kresse G and Hafner J 1994 *Phys. Rev. B* **49** 14251
[48] Kresse G and Furthmüller J 1996 *Phys. Rev. B* **54** 11169
[49] Blochl P, Blöchl E and Blöchl P E 1994 *Phys. Rev. B* **50** 17953
[50] Perdew J P, Burke K and Ernzerhof M 1996 *Phys. Rev. Lett.* **77** 3865
[51] Kohn W and Sham L J 1965 *Phys. Rev.* **140** A1133
[52] Monkhorst H J 1977 *Phys. Rev. B: Condens. Matter* **16** 1748
[53] Wang J, Liu J, Zhang B, Wan H, Li Z, Ji X, Xu K, Chen C, Zha D and Miao L 2017 *Nano Energy* **42** 98
[54] Zhang X R and Liu Y W 2018 *Chin. Phys. B* **27** 014401